A New Facility and Technique for Two-Dimensional Aerodynamic Testing

John B. McDevitt,* Thomas E. Polek,† and Lawrence A. Hand‡
NASA Ames Research Center, Moffett Field, California

The design and operational characteristics of a new test leg for the High Reynolds Number Facility at Ames Research Center are presented, and the unique features of a test section for obtaining two-dimensional airfoil data are reviewed. The new facility operates at unit Reynolds numbers in the range of (1-30) $\times 10^6$/ft. Boundary-layer suction panels are used in the test section (16 in. wide by 24 in. high) to minimize sidewall interference effects. Flexible, easily adjustable upper and lower walls allow test-channel area-ruling so as to nullify Mach number changes induced by mass removal, to correct for longitudinal boundary-layer growth, and to provide contouring compatible with the streamlines of the model in free air.

Nomenclature

A	= channel cross-sectional area
c	= airfoil chord
b,w	= test section width
c_f	= skin friction coefficient
C_p	= pressure coefficient $= (p-p_\infty)/q_\infty$
h	= test-section height
$\dot{m}$	= mass-flow rate
M	= Mach number
p	= static pressure
p_t	= pitot pressure
p_T	= total pressure
q	= dynamic pressure
Re	= Reynolds number
$Re_{c,\infty}$	= Reynolds number based on airfoil chord length and freestream conditions
T	= temperature
u,U	= velocity
x	= streamwise coordinate measured from airfoil leading edge
X	= tunnel longitudinal station (see Fig. 5)
y	= distance from wall
Z	= upper or lower wall coordinate (see Fig. 5)
α	= angle of attack
$\Delta(\ )$	= incremental quantity
δ	= boundary-layer thickness
δ^*	= boundary-layer displacement thickness
δ_0^*	= displacement thickness with zero mass removal
λ_1, λ_2	= test section width and height parameters, respectively
$\langle(\ )\rangle$	= rms value

Subscripts

c	= airfoil chord
e	= edge of boundary layer
N	= nominal value
T	= tunnel or total value
TS	= test section
w	= wall
∞	= freestream conditions
$1,2$	= boundary layer removal systems 1 and 2 (see Fig. 5)

Introduction

THE rapidly expanding computer technology of this era has stimulated such rapid advances in computational fluid dynamics that computers are now routinely used to complement the wind tunnel in the development of new aerospace vehicles. However, continued development of computational methods relies on experimental studies to provide better turbulence models and test cases for evaluating new numerical techniques. As part of a concerted effort at Ames Research Center to advance numerical methods, a new facility, the High Reynolds Number Channel No. 1 (HRC-1) was acquired.[1] An important feature in the design of this facility was the provision for the use of interchangeable test sections; as a result, each basic research study can be as free as possible from restraints on tunnel geometry, and the use of sophisticated techniques for nonintrusive flow measurements and flow visualization can be readily accommodated.

Shortly after the new facility became fully operational in 1975, the Underground Air Storage Facility was constructed at Ames Research Center to provide large quantities of dry high-pressure air for certain Space Shuttle "plume" tests. The availability of this high-pressure storage, which can supply air at mass-flow rates up to 1000 lb/s, (more than twice that originally available) prompted the design and construction of a new and considerably larger test leg HRC-2. This latter channel is described in this paper together with details of a unique test section to be used for the first experimental study—the documentation of subsonic and supercritical flows about two-dimensional airfoils.

The ability to resolve Reynolds number effects is critically important in airfoil testing and the desire for the largest test model possible conflicts with the need to keep wall-interference effects small. Two-dimensional airfoil tests in the past have been plagued with uncertain, and probably large, wall-interference effects. The finite height of the tunnel introduces blockage and restricts streamline curvature. Ventilated walls alleviate blockage but interference effects remain unknown and the walls are difficult, if not impossible, to model numerically. Usually, the test results are assigned "corrected" Mach numbers and angles of attack (see, e.g., Ref. 2). Sidewall interference effects are another source of error (see, e.g., Refs. 3 and 4). An example of noticeable reductions in lift at subsonic speeds because of sidewall boundary layer is presented in Fig. 1.

In the test-section design described in the present paper, suction panels are used to thin the sidewall boundary layers, and flexible, adjustable upper and lower walls are used to avoid blockage and streamline curvature restrictions, and to allow test-channel area-ruling to offset Mach number changes and gradients associated with boundary-layer removal or growth.

Presented as Paper 82-0608 at the AIAA 12th Aerodynamic Testing Conference, Williamsburg, Va., March 22-24, 1982; submitted March 31, 1982; revision received Oct. 8, 1982.

*Research Scientist.
†Facility Manager.
‡Research Scientist. Member AIAA.

Facility Design

Two basic considerations were involved in the preliminary design phase of HRC-2. First, it was decided that the design should permit interchangeable test sections so that each basic research study could be as free as possible from restraints on tunnel geometry. Second, the widest range possible in Reynolds number, consistent with the maximum mass-flow rate available, was desired. In the design study the characteristic length for determining the optimum facility cross-sectional size was related to the chord length c for typical two-dimensional airfoil studies. (It was reasoned that most of the basic fluid dynamics studies in a given facility probably would have characteristic lengths of boundary-layer growth considerably greater than that for airfoils and, comparably, greater Reynolds number ranges.) Airfoil experiments of greatest interest for advancing turbulence modeling concepts are those involving supercritical flows with the attendant, complex shock wave boundary-layer interactions, including separation effects for both steady and unsteady flows.

A nominal test Mach number of $M_\infty = 0.8$ was chosen for the design study, and estimates for the maximum tunnel mass-flow rate $\dot{m}$ were then made. The availability of the new Underground Air Storage Facility allows a maximum flow rate of $\dot{m}_{\max} = 1000$ lb/s. For two-dimensional airfoils spanning the test section, the appropriate test-section cross-sectional shape is rectangular; the width is $\lambda_1 c$ and the height is $\lambda_2 c$ (where c is the airfoil chord). The ratio of λ_2 to λ_1 was chosen to be 3:2; as a result, the test section size may be related to model size as follows:

$$A_{TS} = (3/2)\lambda_1^2 c^2 \qquad \text{(in.}^2\text{)} \tag{1}$$

and the total pressure and Reynolds number based on chord length may be expressed as (for $M_\infty = 0.8$, $T_\infty = 460°$R):

$$p_{t_1} = 29.6(\dot{m}_T/\lambda_1^2 c^2) \qquad \text{(lb/in.}^2\text{)} \tag{2}$$

$$Re_{c,\infty} = 0.863(\dot{m}_T/\lambda_1^2 c) \times 10^6 \tag{3}$$

where $\dot{m}_T$ is the mass-flow rate of the tunnel in pounds per second.

Since airfoil tests at angles of attack were planned, the width parameter λ_1 should be as large as possible. However, boundary-layer suction to thin the boundary layer is included in the test-section design and a value of $\lambda_1 = 2$ was considered adequate. The variations indicated by Eqs. (2) and (3) for the design conditions (maximum mass-flow rate) are shown in Fig. 2. The smallest feasible chord length c (and thus the smallest tunnel) is desired in order to maximize the Reynolds number. However, practical considerations, such as instrumentation, model stress limitations, and model surface roughness, suggest as large a model as possible. The limit for unit Reynolds number of about $(40\text{-}50) \times 10^6$, as shown in Fig. 2, results if the surface roughness is required to be much smaller than the height of the laminar sublayer. The sublayer thickness may be estimated from

$$y^+ = \frac{y(\tau_w/\rho_w)^{1/2}}{\nu_w} \tag{4}$$

where

$$\tau_w = \tfrac{1}{2}\rho_e u_e^2 C_f \qquad C_f/2 = 0.0296/Re^{1/5}$$

For the present application ($M \approx 1, T_e \approx 460°$R), the sublayer thickness y may be approximated by $y^+ = 12$; then

$$y/l = 70/Re^{0.9}$$

Since y is a weak function of boundary-layer run l at high Reynolds numbers, we will consider $l = c/2$; the variation of sublayer thickness with model size (and thus with tunnel size) is displayed in Fig. 3 together with the unit Reynolds number variation (from Fig. 2). The test model can be expected to

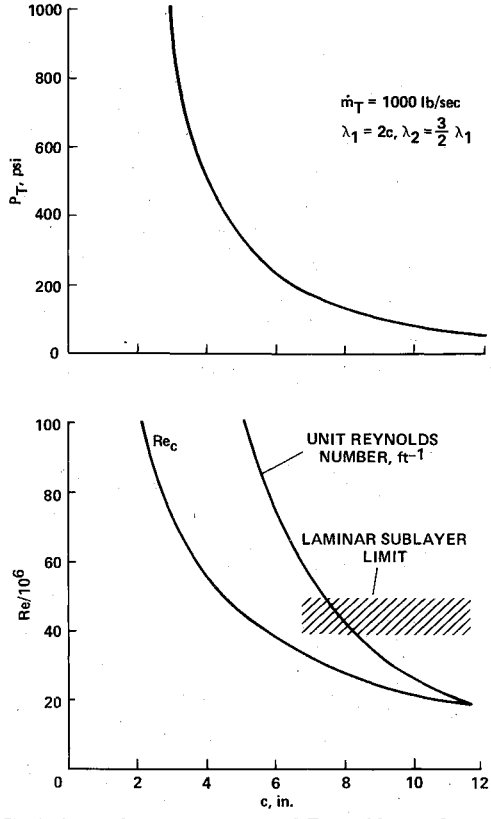

Fig. 2 Variations of total pressure and Reynolds number with test-section size: $M_\infty = 0.8$, $T_\infty = 460°$R.

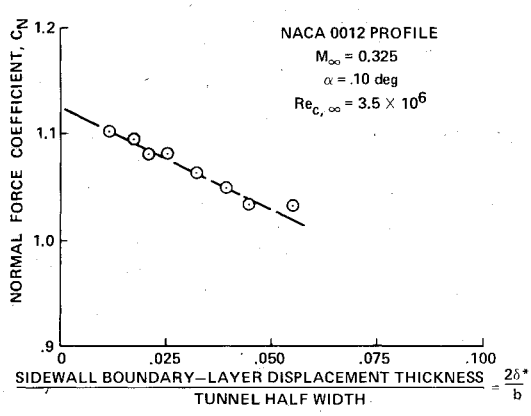

Fig. 1 Reduction in normal force owing to presence of sidewall boundary layer (reproduced from Ref. 3).

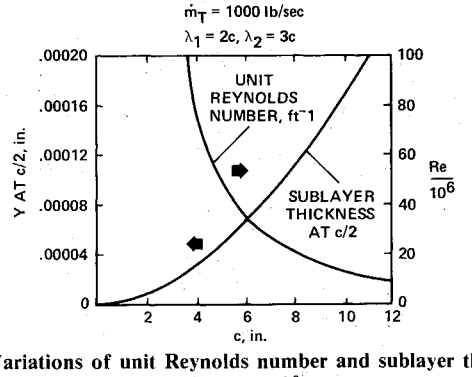

Fig. 3 Variations of unit Reynolds number and sublayer thickness with test-section size: $M_\infty = 0.8$, $T_\infty = 460°$R.

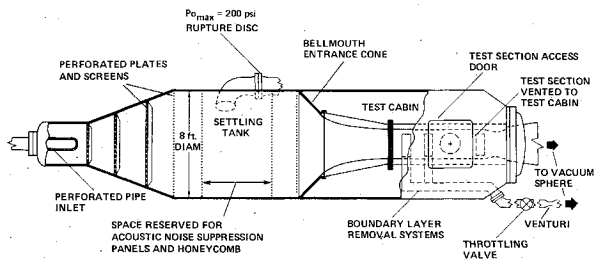

Fig. 4 Schematic of HRC-2 and airfoil test section.

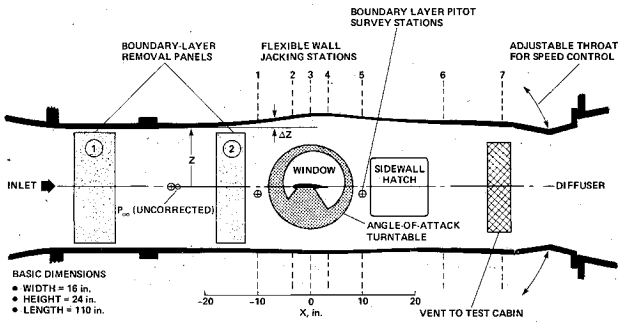

Fig. 5 Airfoil test section for HRC-2.

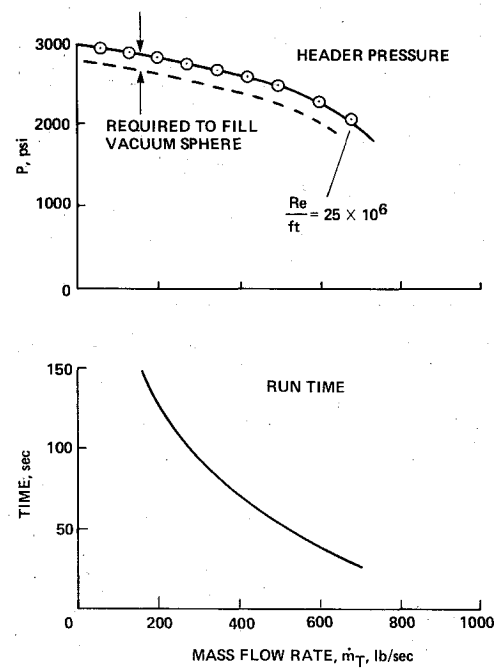

Fig. 6 Variation of supply pressure and available run time with mass-flow rate.

have a surface roughness of from 10 to 20 μin. if care is taken. If the surface roughness effects are to be suppressed, the sublayer height should be equivalent to at least 100 μin., and this leads to the sublayer limit shown in Fig. 2. A chord length of 8 in. is then a reasonable choice for airfoil experiments. This sizes the test section to be 16 in. wide by 24 in. deep. The unit Reynolds number is about 40×10^6 at the design $\dot{m}_{max}$, with a corresponding chord Reynolds number of 27×10^6.

A schematic of the new facility is shown in Fig. 4, and details of the airfoil test section are presented in Fig. 5. The test Mach number is controlled by the adjustable throat at the downstream end of the test section. Sidewall vent panels (perforated plates) just upstream of this throat are located so that the "test cabin" pressure is essentially at freestream static pressure. This alleviates the structural strength and rigidity requirements for the test-section walls and facilitates the use of large viewing ports for shadowgraphs and laser velocimeter measurements. Upper and lower wall-interference effects on the airfoil flowfield are eliminated, at least in principle, by contouring the flexible walls to follow the streamlines in free air at the specific test condition. Numerical flow simulation codes are now available that are adequate for this purpose, provided that the walls are not in the near flowfield of the model (closer than about 1.5 airfoil chord lengths). Sidewall interference effects are to be minimized by thinning the sidewall boundary layer by suction at two sets of porous panels (one set near the entrance to the test section and the other near the model), each set operating separately from the other. The suction is provided by the low pressure in the downstream vacuum sphere; the mass-removal rate is controlled by throttling valves and monitored at venturi sections (see lower-right-hand portion of Fig. 4). The porous panels consist of 0.25-in.-thick sheets of sintered stainless steel fibers (Feltmetal No. FM 1312, Brunswick Corp., Technetics Division) backed by a 0.25-in.-thick perforated plate (50% open).

The test section was made sufficiently long that the upper and lower walls might be replaced, sometime in the future, with slotted or perforated walls for transonic operation [the lengths of transonic test sections are typically $5(A_{TS})^{1/2}$]. Provision was also made for two additional flow-bypass systems (similar to those for test-section boundary-layer removal) for separate control of upper and lower plenum chamber pressures, if operated transonically.

The source of high-pressure dry air is the 33,000-ft^3 Ames Underground Air Storage Facility, pressurized to 3000 psi and maintained at ambient temperature. The High Reynolds Number Facility is connected to the storage facility by a high-pressure pipe in which the pressure drops with mass-flow rate, as shown in Fig. 6. Although the header pressure decreases rapidly with increasing mass-flow rate, the available total head remains much larger than required (see Fig. 2 for $c=8$ in.). These measurements indicate that the maximum mass-flow rate will be about 800 lb/s; with the present test section, unit Reynolds numbers up to about 30×10^6/ft can be achieved and airfoil test data can be acquired in the Reynolds number range (based on chord length) from about 1×10^6 to 20×10^6. The facility discharges into a large "vacuum sphere," and the run time at high mass-flow rates is essentially limited by the time required to fill this sphere to 25 psia, as shown in Fig. 6.

Freestream Turbulence Measurements

High-frequency pressure transducers and hot wire anemometers were used to measure pressure and velocity fluctuations in the test section. Typical results are presented in Table 1. Space has been reserved in the settling tank (Fig. 4) for the future use of acoustic noise suppression panels and honeycomb section.

Test-Section Calibration

The calibration of the test section was performed basically in two phases. First, an evaluation was made of the effectiveness of the porous suction panels for thinning the sidewall boundary layers. Second, both the effects of boundary-layer growth and of mass removal on Mach number

Table 1 Test-section pressure and velocity levels,[a] $M_\infty = 0.8$

P_T, psia	$\langle P\rangle/q_\infty$	$\langle u\rangle/U_\infty$
20	0.02	0.0046
40	0.02	0.0050

[a]Measurements by F. K. Owen of Complere, Inc.; NASA Contract NAS2-10859.

distributions were determined in order that the flexible upper and lower walls could be adjusted so as to nullify these effects as much as possible.

The performances of the two boundary-layer removal systems were evaluated from pitot-pressure rate surveys at three sidewall stations ($X = -25$, -10, and $+10$) (see Fig. 5). Typical measurements of boundary-layer displacement thickness, normalized with respect to that for no mass removal, δ_0^*, are presented in Fig. 7 for each system operating independently. Typical surveys with both systems operating are shown in Fig. 8 and the effect of mass removal on displacement thickness summarized in Fig. 9. Longitudinal variations in displacement thickness are shown in Fig. 10. The present technique for thinning the sidewall boundary layer (and thus reducing wall-interference effects) was considered to be very successful, since the displacement thickness was reduced by at least 70% at the airfoil test station.

The effects of longitudinal boundary-layer growth in the test channel and local flowfield changes due to the operation of boundary-layer removal system 2 will be considered next (system 1 is far enough upstream as to be unimportant in this regard). Typical longitudinal Mach number distributions, as deduced from sidewall pressure measurements, are shown in Fig. 11. For these tests, the upper and lower walls were parallel, as were the nonmovable sidewalls, and the Mach number gradient at the airfoil test station ($X=0$) may be related to the boundary-layer growth, as illustrated in Fig. 12. Values for $\partial\delta^*/\partial X$, as deduced from measured values of

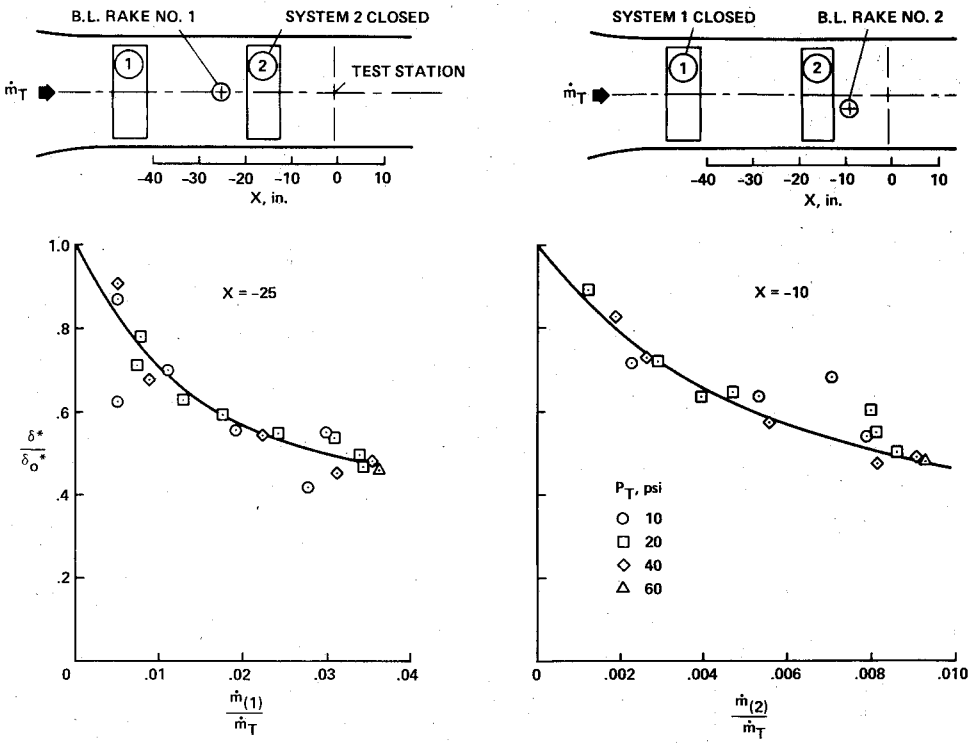

Fig. 7 Performances of boundary-layer removal systems 1 and 2 operating individually.

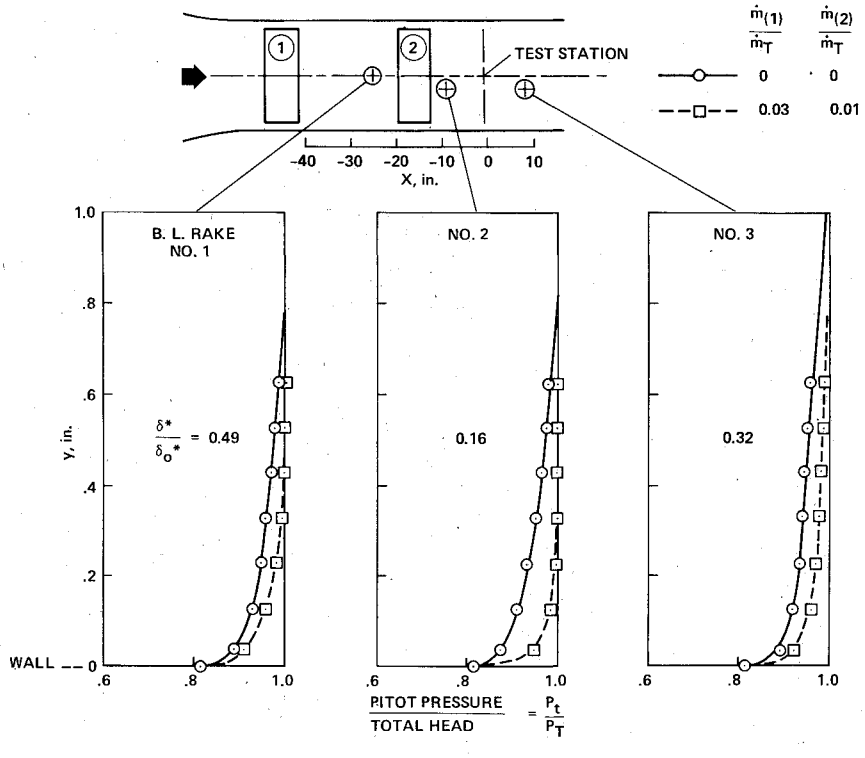

Fig. 8 Typical boundary-layer pitot surveys with both systems operating: $M_N = 0.6$, $P_T = 20$ psi.

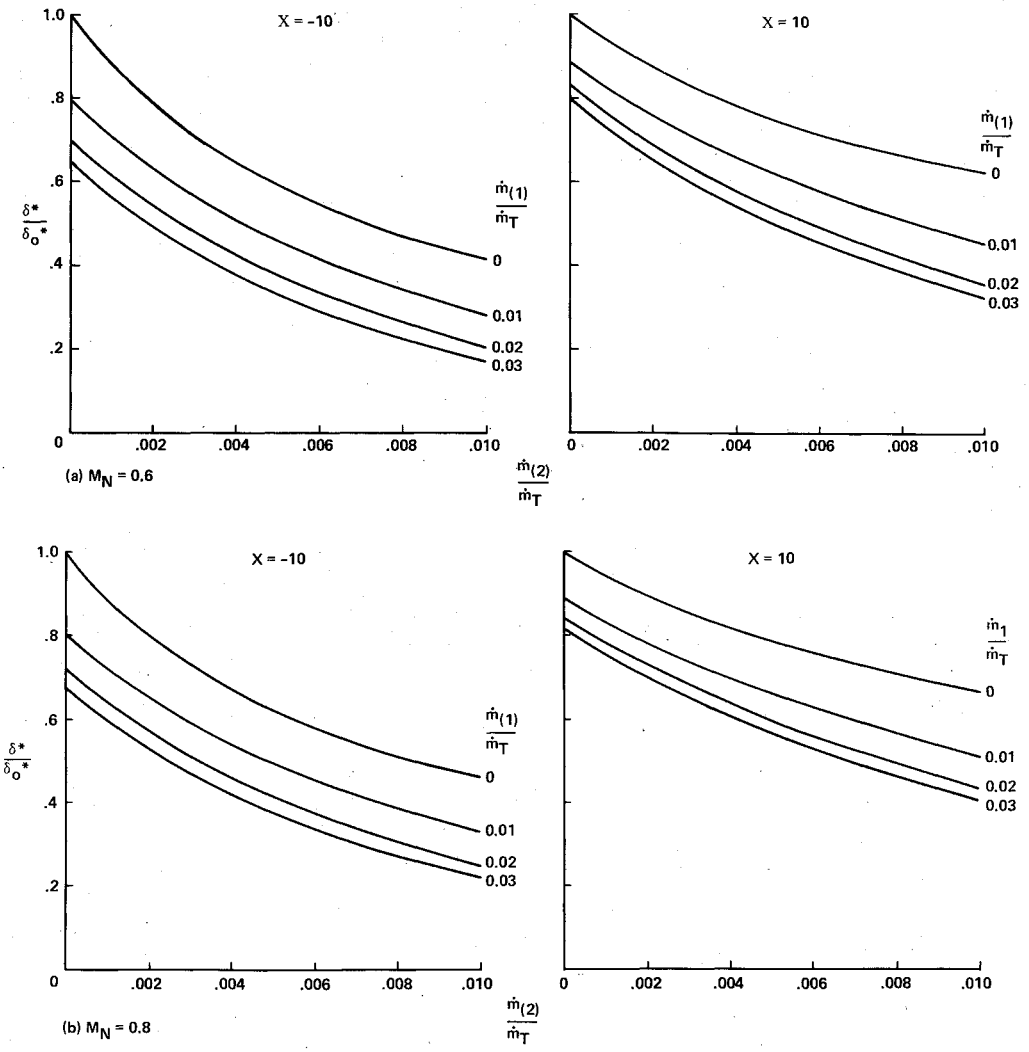

Fig. 9 Sidewall boundary-layer displacement thickness variations with both mass-removal systems operating: $P_T = 20$ psi.

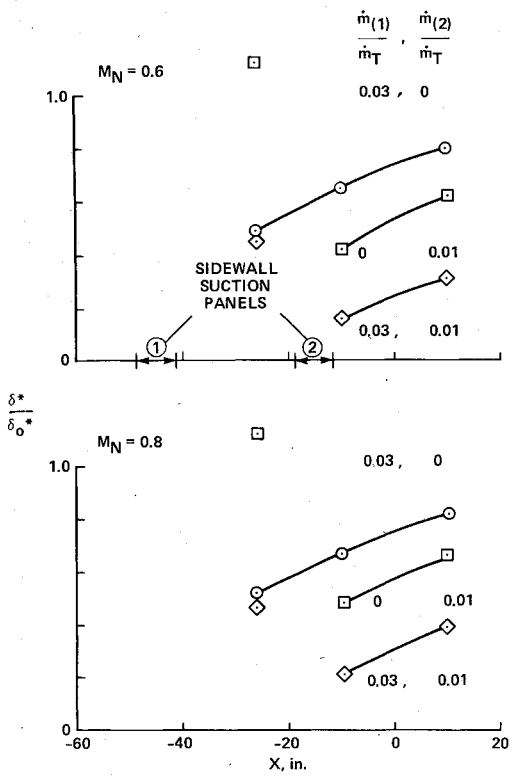

Fig. 10 Typical longitudinal variations in boundary-layer displacement thickness: $P_T = 20$ psi.

$\partial M/\partial X$ at $X=0$, are presented in Fig. 13. A mean value of $\partial\delta^*/\partial X = 0.0027$ was chosen and a ramp angle of $5/2[\tan^{-1} 0.0027 = 0.16 \text{ deg}] = 0.39$ deg used to set the upper and lower walls as a boundary-layer growth correction near the model testing station ($X=0$). The flexible wall setting used is shown at the top of Fig. 14; the desired result of essentially zero longitudinal Mach number gradients near the test station was obtained (compare Figs. 11 and 14).

The undesirable local Mach number changes associated with the use of boundary-layer removal system 2 were eliminated as follows: First, the Mach number increment

$$\Delta M = M_{X=10} - M_{X=-24}$$

was determined (Fig. 15). It was then assumed that associated with each ΔM is an incremental area change ΔA; the result of analyzing a large number of calibration runs is shown in Fig. 16. The effect of mass removal on channel cross-sectional area is illustrated schematically in Fig. 17; to minimize Mach number effects, the channel should be reshaped so that $A_1 = A_2$. In the present case, the flexible upper and lower walls will be used for this purpose.

Referring to Fig. 16, an area change of 1.5% is associated with a mass-removal rate of about 1% at a nominal Mach number of 0.8 (point A). This correction, together with the boundary-layer growth correction previously discussed, was applied as shown in the sketch at the top of Fig. 18. The desired result was obtained. [Compare Figs. 14 and 18 (of course, the data for no mass removal, $\dot{m}_2 = 0$, now reflect an improper channel area ruling).]

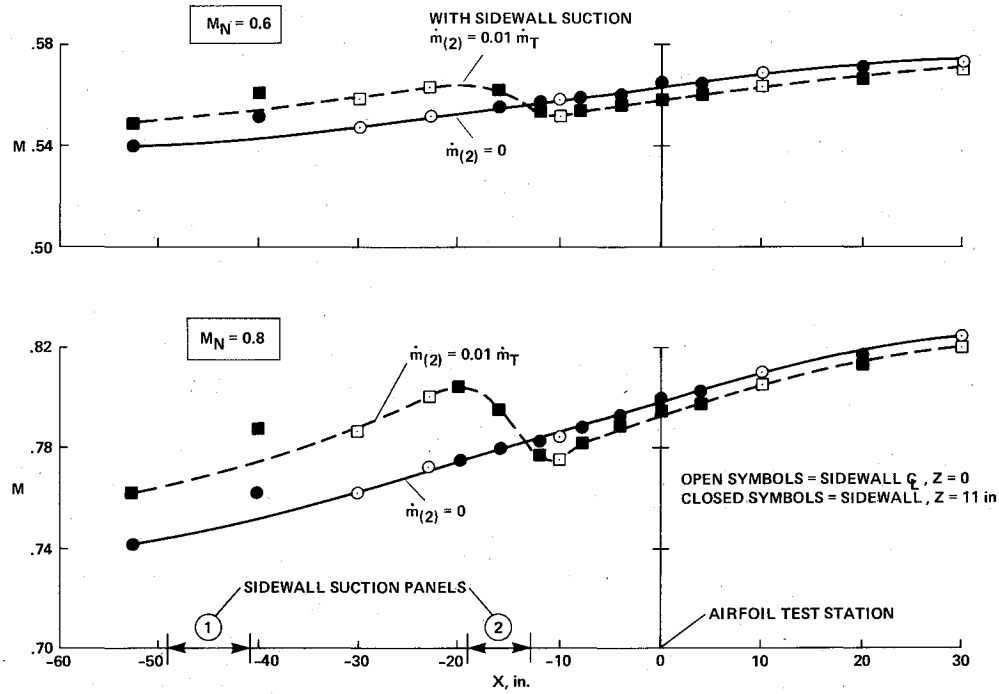

Fig. 11 Effect of boundary-layer removal system 2 on longitudinal Mach number distribution: $P_T = 20$ psi.

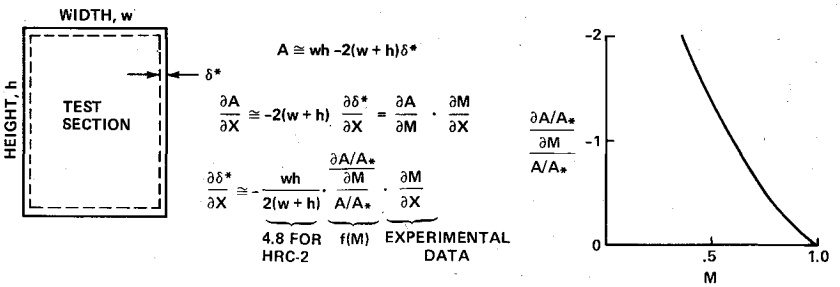

Fig. 12 Relationship between Mach number gradient and boundary-layer growth.

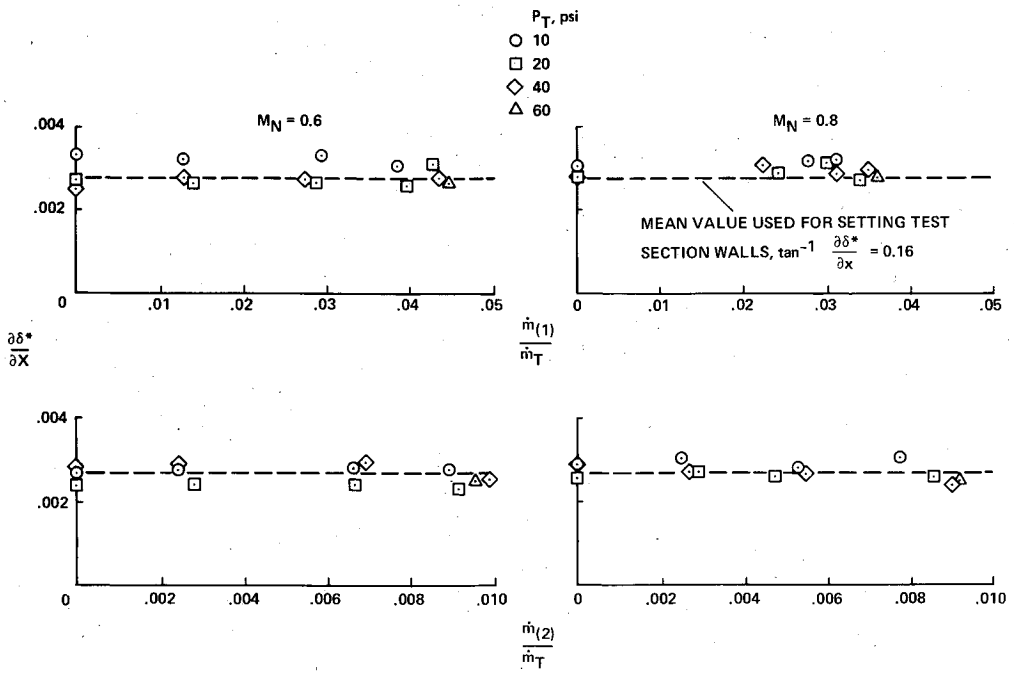

Fig. 13 Boundary-layer growth as deduced from measured $\partial M/\partial X$.

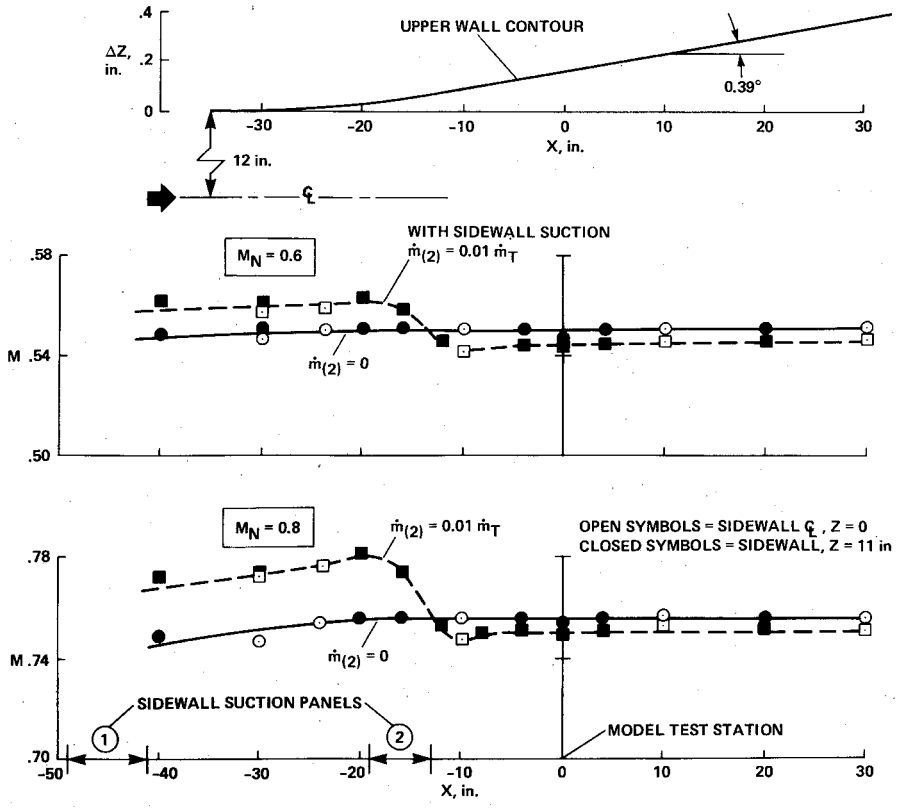

Fig. 14 Longitudinal Mach number distributions with upper and lower walls diverged 0.39 deg (to correct for boundary-layer growth).

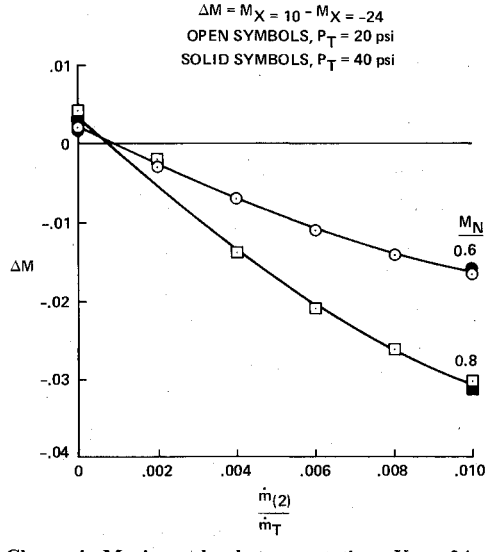

Fig. 15 Change in Mach number between stations $X = -24$ and $+10$ with the upper and lower walls diverged 0.39 deg.

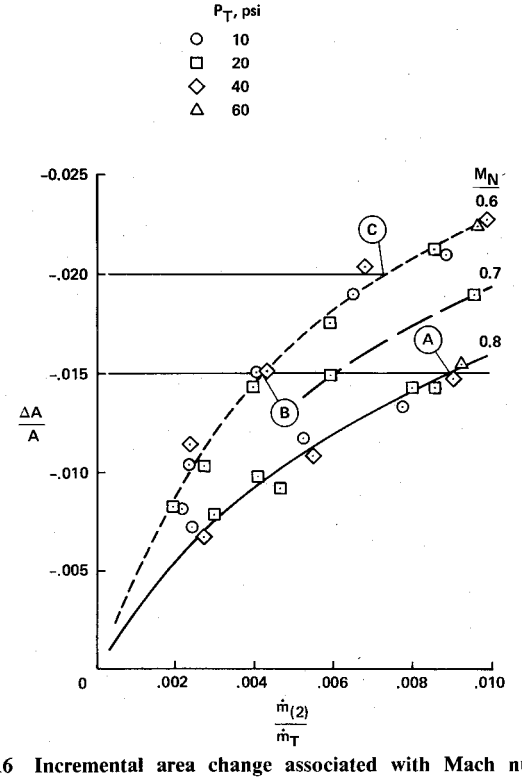

Fig. 16 Incremental area change associated with Mach number change.

The changes in Mach number between stations $X = -24$ and 10 are shown in Fig. 19 for area changes of 1.5% and 2%. Labels A, B, and C correspond to similar labels in Fig. 16. For $\Delta A/A = -0.015$ (Fig. 16) the Mach number increment ΔM should be zero for $M_N = 0.8$ when $\dot{m}_2 = 0.009$ (point A) and zero for $M_N = 0.6$ when $\dot{m}_2 = 0.0043$ (point B). The measurements shown in Fig. 19 reflect this closely. For $\Delta A/A = -0.02$ (Fig. 16), the area change is always too large at $M_N = 0.8$ (for $\dot{m}_2 \leq 0.01$) but is the proper value at $M_N = 0.6$ when $\dot{m}_2 = 0.0075$ (point C) and the measured Mach number was zero at that point (see Fig. 19). These experiments demonstrate that the undesirable longitudinal Mach number changes induced by sidewall mass removal can be essentially eliminated by internal area ruling.

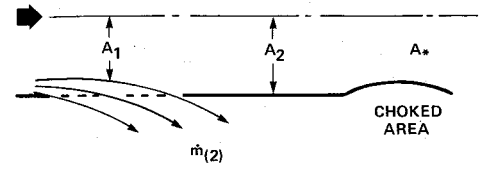

Fig. 17 Schematic of channel area change with mass removal.

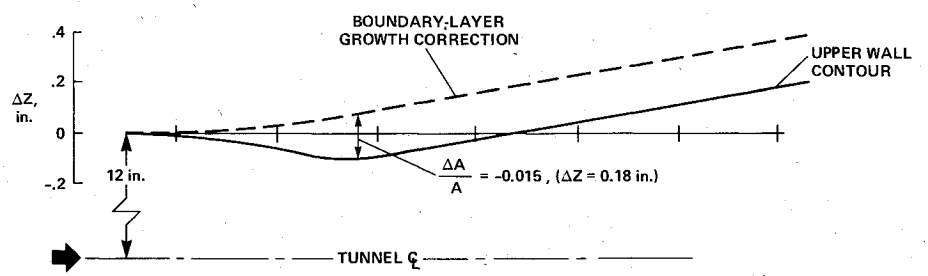

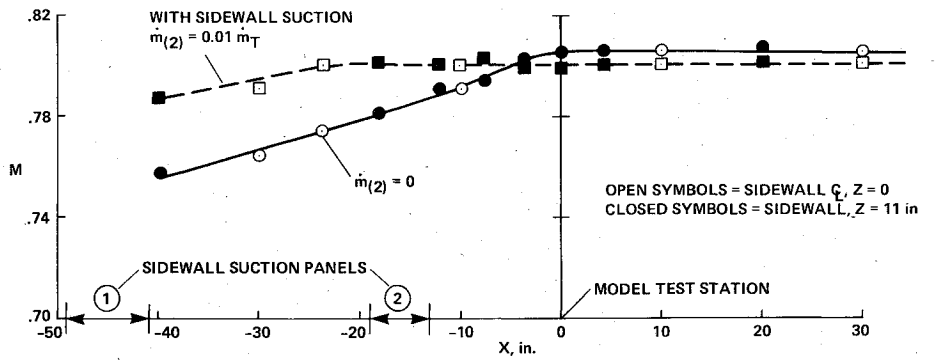

Fig. 18 Longitudinal Mach number distributions with upper and lower walls shaped to correct for both boundary-layer growth and mass removal ($\Delta A/A = 0.015$): $M_N = 0.8$, $P_T = 20$ psi.

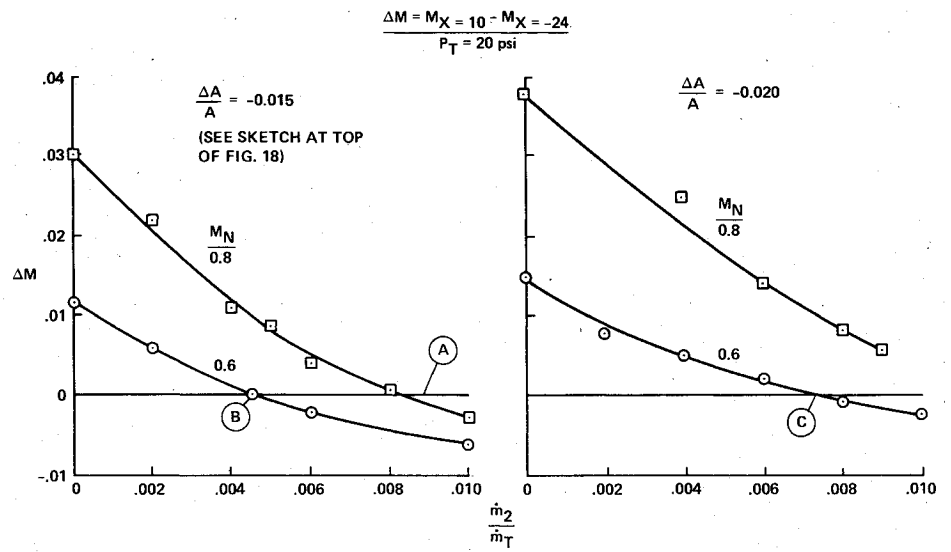

Fig. 19 Mach number change between stations $X = -24$ and $+10$ when the upper and lower walls are shaped to correct for boundary-layer growth and for mass-removal area changes of 1.5% and 2%.

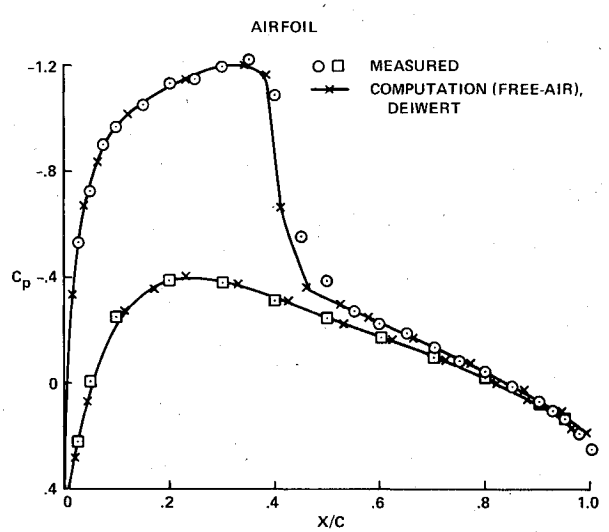

SIDEWALL (MEASURED)

X	Cp Z = 11	Cp Z = 0	Cp Z − 11
-30	0.035	0.057	0.045
-24		0.010	
-20	-0.014		
-16	-0.012		
-12	-0.008		
-10		0.059	
-8	-0.048		-0.004
-4	-0.096		0.019
0	-0.058		0.004
4	-0.071		-0.005
8	-0.019		-0.004
10		0.034	
12	-0.001		0.020
16	-0.009		0.014
20	-0.003		0.031
30	0.027	0.027	0.036

Fig. 20 Experimental and calculated surface-pressure distributions for a NACA 0012 profile: $M_\infty = 0.75$, $\alpha = 2$ deg, $Re_{c,\infty} = 10^7$.

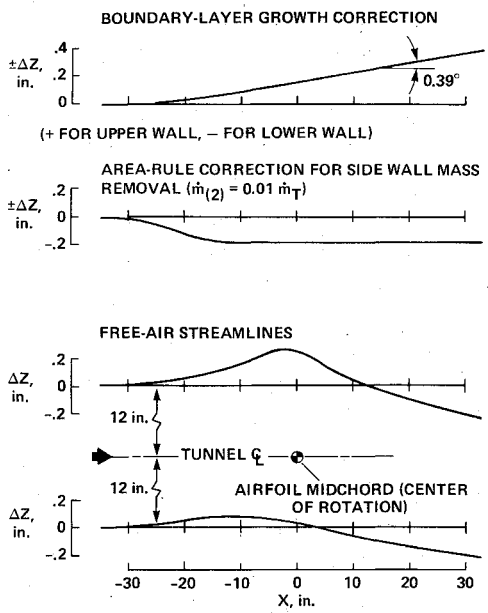

Fig. 21 Wall contours used to obtain the test data of Fig. 20.

Airfoil Testing

As part of the overall checkout and calibration of the new facility, a limited airfoil test program was included. An unswept NACA 0012 airfoil with a chord of 8 in., spanning the tunnel, was chosen for this purpose. An example of measured airfoil pressure coefficients is presented in Fig. 20. This test was conducted at $M_\infty = 0.75$ and $\alpha = 2$ deg, which is slightly below the buffet boundary, and the upper embedded supersonic flow zone extends about halfway to the tunnel ceiling. The sidewall boundary-layer removal systems were operated at $\dot{m}_1 = 0.03\dot{m}_T$ and $\dot{m}_2 = 0.01\dot{m}_T$ ($\dot{m}_T$ = tunnel mass-flow rate). The flexible upper and lower walls were set as shown in Fig. 21 to compensate for boundary-layer growth, sidewall mass removal, and to follow free-air streamlines, as calculated by the numerical method of Deiwert.[5,6] (Deiwert's method is an airfoil computational method that solves the time-dependent two-dimensional Reynolds-averaged Navier-Stokes equations with simple algebraic eddy-viscosity models.)

The freestream test Mach number M_∞ was determined from a sidewall pressure measurement at $X = -24$ and by then applying three small corrections to the Mach number: 1) the Mach number was reduced by 0.003, to more nearly represent the flow in the central region of the test channel; 2) reduced an additional 0.003 for the longitudinal correction (from calibration data similar to those in Fig. 19); and 3) increased by 0.0050 to offset the influence of the downstream presence of the model (estimated by Deiwert's numerical method). In this particular case the three small corrections nearly cancel out. In this example there was no need to correct the test angle of attack or Mach number, for the measurements are essentially free of wall-interference effects, and very good agreement was obtained between experiment and predicted values for the model in free air.

Concluding Remarks

The design and operational characteristics of a new test leg for the High Reynolds Number Facility at Ames Research Center and the unique features of a test section for obtaining two-dimensional airfoil data have been reviewed. It has been demonstrated that the sidewall boundary-layer displacement thickness approaching the model can be reduced by at least 70% and that test-channel internal area-ruling can be used to nullify both the Mach number changes introduced by sidewall suction and the gradients caused by natural boundary-layer growth (thus avoiding "buoyancy" effects). Flexible upper and lower test-channel walls were used to provide the proper longitudinal area distribution and to achieve contouring compatible with streamlines for the test model in free air.

The capability of significantly thinning the sidewall boundary layer, the use of easily adjustable upper and lower walls (to minimize wall-interference effects), and the capability to operate over a wide range of Reynolds numbers insures that this new facility will have an exciting and productive future. The first research studies planned for the facility involve the documentation of steady and unsteady (buffeting) flowfields about NACA 0012 and Korn-Garabedian airfoils and an evaluation of wall-interference phenomena during airfoil testing. The primary purpose for conducting these tests is to acquire well-documented flowfields suitable for the critical evaluation of airfoil codes, with particular attention directed toward turbulence-modeling concepts. Since solid upper and lower walls are used, representative boundary conditions (tangential flow at the walls) can easily be included in the numerical methods and comparisons of solutions with and without wall boundary conditions used to monitor wall-interference effects. It is not necessary, of course, to use free-air data to evaluate codes, but this is to be preferred in order to avoid dealing with the uncertainties of wall-interference effects. The extensive role of the computer in the airfoil test procedure described in this paper should not be misinterpreted—the computer cannot be used to direct research, but it is invaluable in helping us define and conduct better experiments.

References

[1] McDevitt, J.B., Levy, L. Jr., and Deiwert, G.S., "Transonic Flow About a Thick Circular-Arc Airfoil," *AIAA Journal,* Vol. 14, May 1976, pp. 606-613.

[2] Barche, J., "Experimental Data Base for Computer Program Assessment," AGARD Advisory Report 138, May 1979.

[3] Bernard-Guelle, R., "Influence of Wind Tunnel Wall Boundary Layers on Two-Dimensional Transonic Tests," NASA TT F17,255 (Translation of "Influence des Couches Limites Laterales de Souffle rie Dans les Essais Transsoniques en Courant Plan," 12th Applied Aerodynamic Colloquium, ENSMA/CEAT, Poitiers, France, Nov. 1975, pp. 1-22).

[4] Sewall, W.G., "The Effects of Sidewall Boundary Layers in Two-Dimensional Subsonic and Transonic Wind Tunnels," AIAA Paper 81-1297, 1981.

[5] Deiwert, G.S., "Numerical Simulation of High Reynolds Number Transonic Flows," *AIAA Journal,* Vol. 13, Oct. 1975, pp. 1354-1359.

[6] Deiwert, G. S., "Computation of Separated Transonic Turbulent Flows," *AIAA Journal,* Vol. 14, June 1976, pp. 735-740.